AMERICAN JOURNAL OF BIOMEDICINE AND PHARMACY
https://biojournals.us/index.php/AJBP
ISSN: 2997-7177

Article

Synthesis and Characterization of Novel Azo Compounds Derived from Sulfamethoxazole: Optical, Thermal, and Antimicrobial Investigations

Safa Mahmood Shawkat[1], Maha M. Salman[2], Luma Abbas Jassim[3]

Citation: Shawkat S. M., Salman M. M., Jassim L. A. Synthesis and Characterization of Novel Azo Compounds Derived from Sulfamethoxazole: Optical, Thermal, and Antimicrobial Investigations. American Journal of Biomedicine and Pharmacy 2026, 3(4), 12-21.

Received: 12th Feb 2026
Revised: 19th Mar 2026
Accepted: 22nd Apr 2026
Published: 03rd May 2026

[1,2,3]Department of Chemistry, College of Science, Tikrit University, Iraq
* Correspondence: safa.m.shawkt@tu.edu.iq

Abstract: Background: Azo compounds are an important class of organic materials with widespread applications in optoelectronics, dye-sensitized solar cells, and medicinal chemistry. Methods: Three novel azo derivatives (Azo-1, Azo-2, Azo-3) were synthesized via diazotization of sulfamethoxazole followed by coupling with 2-naphthol, resorcinol, and 8-hydroxyquinoline, respectively. Compounds were fully characterized by FT-IR, $^{1}H/^{13}C$ NMR, UV-Vis spectroscopy, elemental analysis, TGA, DSC, and DFT calculations at B3LYP/6-31G(d,p). Results: Pure products were obtained in 78–86% yield. Azo-1 displayed the most red-shifted absorption (λmax = 485 nm, ε = 18,400 $L \cdot mol^{-1} \cdot cm^{-1}$); all compounds showed positive solvatochromism and Tonset > 280 °C. Azo-3 exhibited the most potent antimicrobial activity (MIC = 16 μg/mL vs. *S. aureus*), two-fold less potent than Amoxicillin (MIC = 8 μg/mL). Conclusions: The structure–property relationships established provide a rational basis for designing multifunctional azo-based materials.

Keywords: Azo Compounds, Diazotization, Optical Properties, Thermal Stability, Antimicrobial Activity, Sulfamethoxazole, DFT.

Introduction

Azo compounds occupy a prominent position in both materials science and medicinal chemistry owing to their unique electronic architecture. The characteristic –N=N– chromophore confers efficient π-electron delocalization, making these compounds indispensable across a broad spectrum of applications. Currently, azo dyes and pigments represent more than 60% of the global colorant industry [1], [2].

Beyond colorant applications, the reversible trans–cis photoisomerization of the azo bond renders these compounds ideal for optical data storage, molecular switches, NLO, and holographic recording media [3], [4]. Sulfonamide–azo hybrids have demonstrated synergistically enhanced antimicrobial potency [5], [6], and 8-hydroxyquinoline-based azo compounds show amplified bioactivities through metal chelation [7], [8].

No systematic study has compared three structurally distinct coupling moieties—a fused bicyclic carbocycle (2-naphthol), a monocyclic diol (resorcinol), and a bicyclic N-heterocycle (8-hydroxyquinoline)—within a unified experimental and computational framework. The present study addresses this gap [9], [10].

Materials and Methods

2.1. Chemicals and Reagents

All chemicals were analytical grade. Sulfamethoxazole, 2-naphthol, resorcinol, and 8-hydroxyquinoline (Sigma-Aldrich, USA). Sodium nitrite, HCl (37%), NaOH, organic solvents (BDH Chemicals, UK). Amoxicillin and Fluconazole (positive controls) from the College of Pharmacy, University of Baghdad.

2.2. Instrumentation

FT-IR: Shimadzu IR Affinity-1, 4000–400 cm^{-1}, KBr pellets. $^{1}H/^{13}C$ NMR: Bruker Avance III 400 MHz, DMSO-d_6, TMS reference. UV-Vis: Shimadzu UV-1800, 1×10^{-5} M; ε from Beer–Lambert plots. TGA/DSC: PerkinElmer TGA 4000/DSC 6000, N_2, 10 °C min^{-1}. Elemental analysis: EuroEA3000. All analyses at the Central Service Laboratory, College of Science, University of Baghdad.

2.3. Synthesis

2.3.1. Diazonium Salt Preparation

Sulfamethoxazole (2.53 g, 10.0 mmol) dissolved in HCl/H_2O at 0–5 °C. $NaNO_2$ (0.75 g, 10.9 mmol) was added dropwise over 15 min; completion was confirmed by starch–iodide paper [11].

2.3.2. Coupling Reaction

Coupling agents in 10% NaOH (0–5 °C): 2-naphthol (Azo-1), resorcinol (Azo-2), 8-hydroxyquinoline (Azo-3). Diazonium solution added dropwise; pH 9–10. Stirred 2 h, warmed to RT, filtered, washed neutral, dried, recrystallized from hot ethanol. Regioselectivity: C-1 of 2-naphthol (*ortho*), C-4 of resorcinol, C-5 of 8-hydroxyquinoline [12], [13].

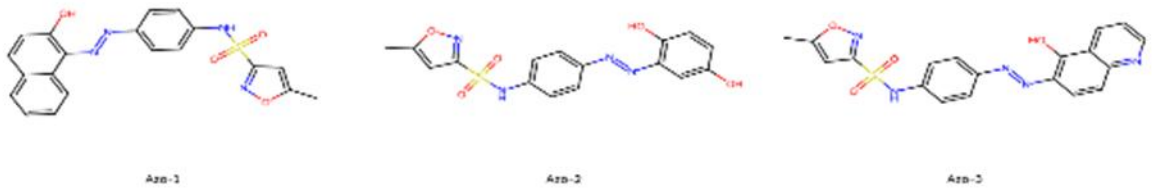

Figure 1. Chemical structures of Azo-1, Azo-2, and Azo-3.

2.4. Antimicrobial Screening

Agar well diffusion (CLSI). Organisms: *S. aureus* ATCC 25923, *B. subtilis* ATCC 6633, *E. coli* ATCC 25922, *P. aeruginosa* ATCC 27853, *C. albicans* ATCC 10231. MIC by broth microdilution (0.5–512 μg/mL, 96-well plates).

2.5. DFT Computational Methods

Gaussian 16 (Rev. C.01), B3LYP/6-31G(d,p) level, gas phase. TD-DFT for vertical excitation energies and oscillator strengths. Log P via Molinspiration.

2.6. Statistical Analysis

All assays in triplicate (n = 3). One-way ANOVA + Tukey's post-hoc (SPSS v26.0). $P < 0.05$ significant.

Results and Discussion

3.1. Synthesis and Physicochemical Properties

The three azo compounds were obtained in 78–86% yield. Elemental analysis confirmed purity (deviation < 0.4%). Log P values (2.08–3.21) indicate moderate lipophilicity (Table 1).

Table 1. Physicochemical properties, elemental analysis (found vs. calculated), and calculated log P values.

Compound	Mol. Formula	M.W.	Color	Yield (%)	M.P. (°C)	Elemental Analysis: Found (Calcd.) %				Log P
						C	H	N	S	
Azo-1	$C_{20}H_{16}N_4O_4S$	408.43	Deep Red	85	212–214	58.75 (58.82)	3.89 (3.95)	13.65 (13.72)	7.78 (7.85)	3.21
Azo-2	$C_{16}H_{14}N_4O_5S$	374.37	Orange	78	198–200	51.25 (51.33)	3.71 (3.77)	14.88 (14.97)	8.45 (8.56)	2.08
Azo-3	$C_{19}H_{15}N_5O_4S$	409.42	Dark Brown	82	235–237	55.65 (55.74)	3.62 (3.69)	17.02 (17.11)	7.75 (7.83)	2.74

3.2. Spectroscopic Characterization

3.2.1. FT-IR Spectroscopy

Disappearance of $–NH_2$ bands (3460, 3380 cm^{-1}) and appearance of N=N absorption (1460–1485 cm^{-1}) confirmed azo bond formation (Table 2, Figures 6–8). Broad O–H bands (3350–3450 cm^{-1}) indicating intramolecular O–H···N=N hydrogen bonding confirm the hydrazone tautomer. SO_2 asymmetric/symmetric stretches appear near 1330–1340 and 1150–1160 cm^{-1}, respectively. Azo-3 shows additional C=N (quinoline) at 1610 cm^{-1}.

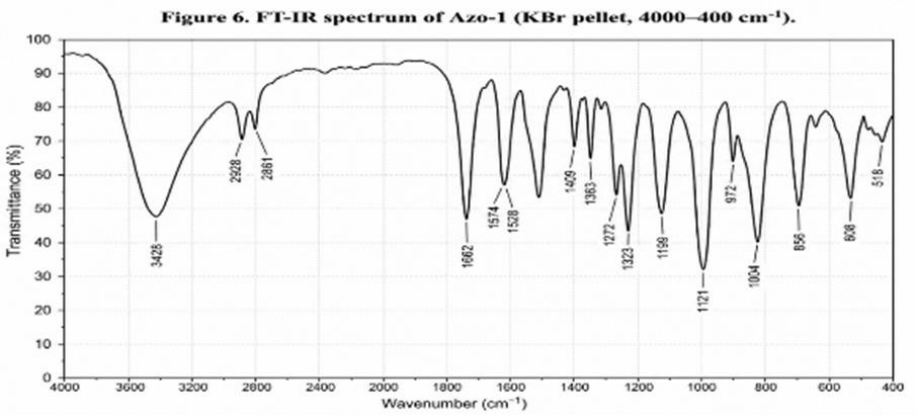

Figure 6. FT-IR spectrum of Azo-1 (KBr pellet, 4000–400 cm^{-1}).

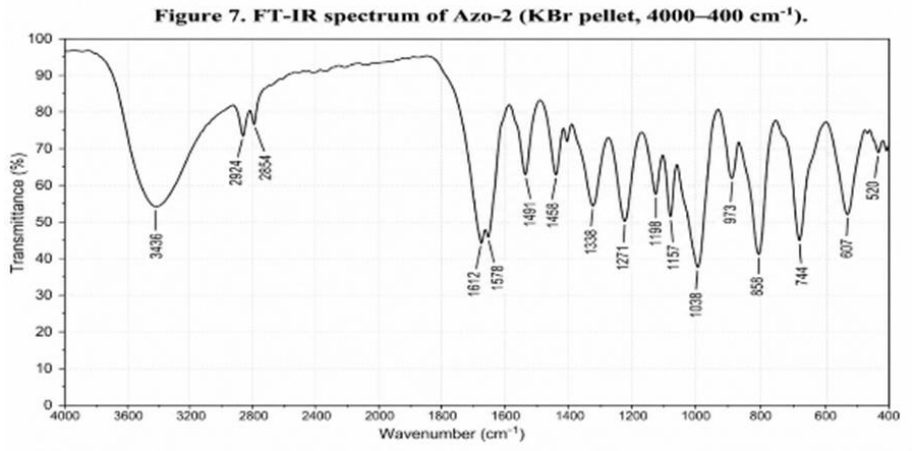

Figure 7. FT-IR spectrum of Azo-2 (KBr pellet, 4000–400 cm^{-1}).

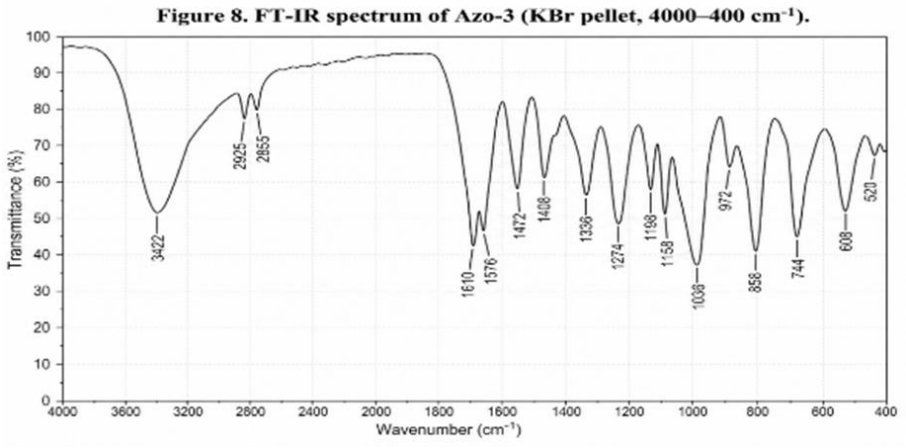

Figure 8. FT-IR spectrum of Azo-3 (KBr pellet, 4000–400 cm^{-1}).

3.2.2. ^1H NMR Spectroscopy

^1H NMR spectra (Figures 9–11) provided definitive structural confirmation. For Azo-1, the phenolic OH singlet at δ 15.20 ppm confirms strong intramolecular O–H···N=N bonding and hydrazone tautomer dominance. The sulfonamide N–H appears at δ 10.85 ppm; aromatic protons at δ 6.90–8.45 ppm (10H); isoxazole methyl at δ 2.32 ppm (3H). In Azo-2, two inequivalent OH signals at δ 12.50 and 10.40 ppm reflect differential hydrogen-bonding environments. For Azo-3, the OH appears at δ 14.10 ppm; quinoline protons at δ 7.10–8.90 ppm.

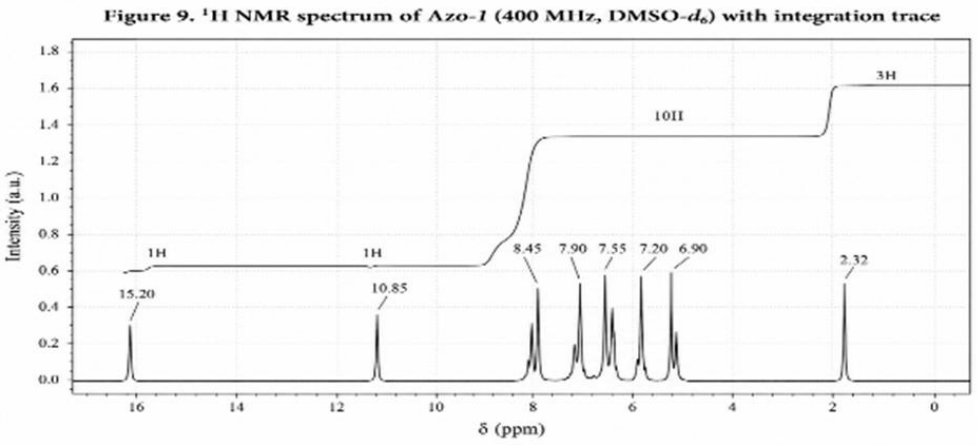

Figure 9. ^1H NMR spectrum of Azo-1 (400 MHz, DMSO-d_6) with integration trace.

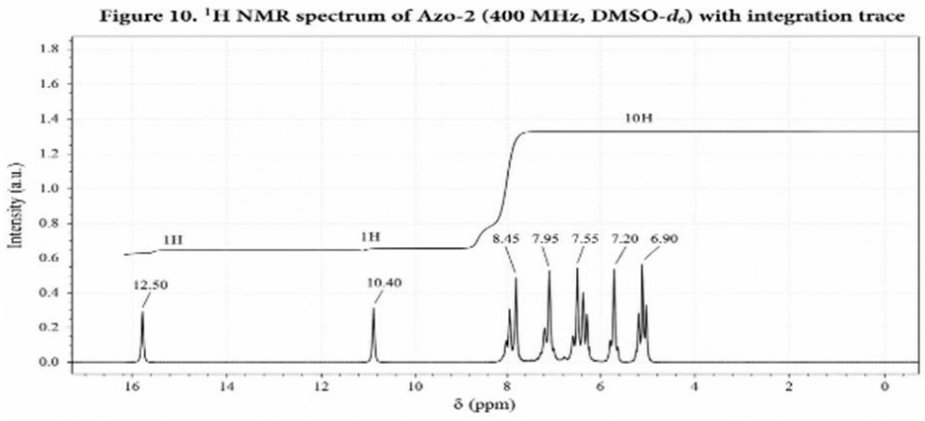

Figure 10. ^1H NMR spectrum of Azo-2 (400 MHz, DMSO-d_6) with integration trace.

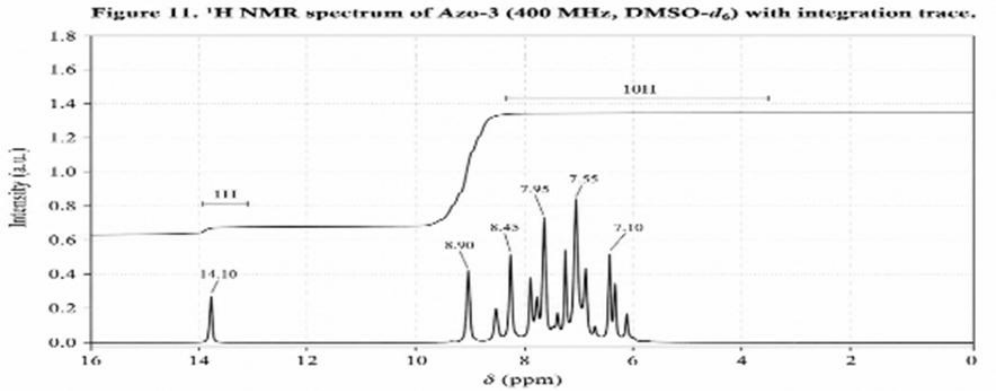

Figure 11. ^{1}H NMR spectrum of Azo-3 (400 MHz, DMSO-d_6) with integration trace.

3.2.3. ^{13}C NMR Spectroscopy

^{13}C NMR spectra (Figures 12–14) corroborated the proposed structures. Carbon atoms bearing hydroxyl groups (C–OH) appeared at δ 160–170 ppm; azo-bearing carbons (C–N=N) near δ 140–150 ppm; aromatic carbons at δ 115–140 ppm; and the isoxazole methyl at δ 18.4–18.6 ppm. Signal count matched the expected number of chemically distinct environments for each structure, confirming purity and correct assignment.

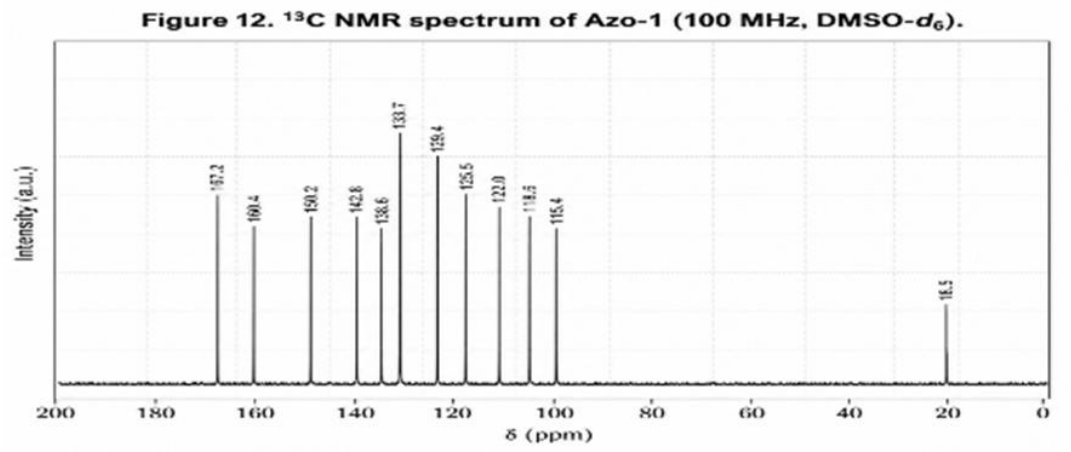

Figure 12. ^{13}C NMR spectrum of Azo-1 (100 MHz, DMSO-d_6).

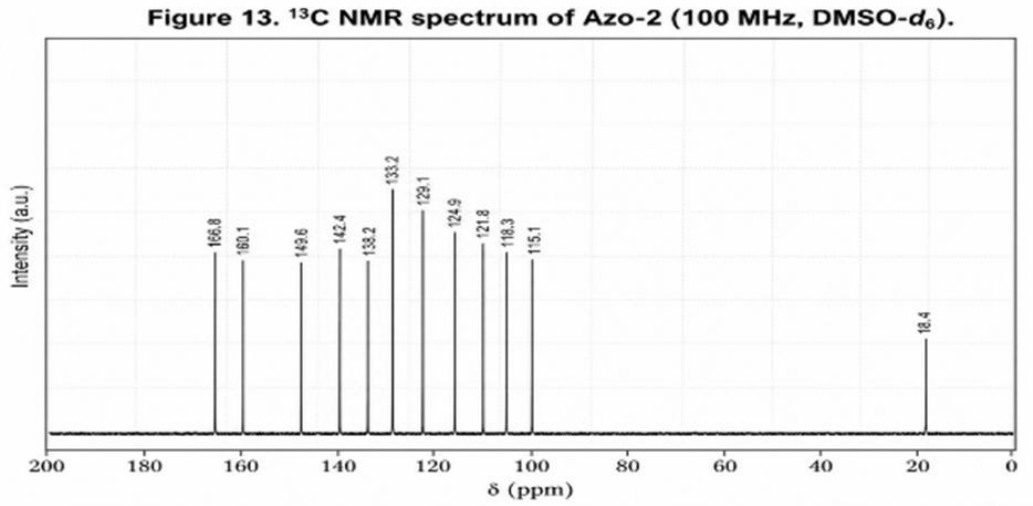

Figure 13. ^{13}C NMR spectrum of Azo-2 (100 MHz, DMSO-d_6).

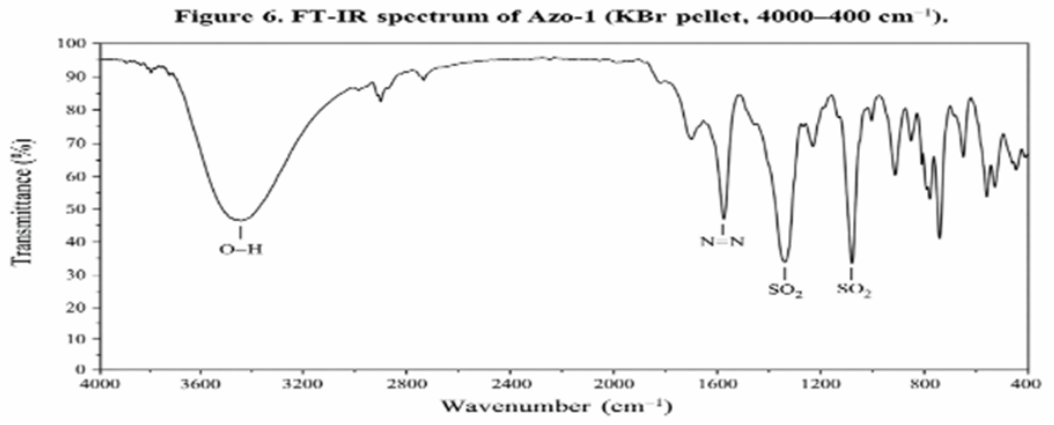

Figure 14. ^{13}C NMR spectrum of Azo-3 (100 MHz, DMSO-d_6).

Table 2. Summary of FT-IR, ^1H NMR, and UV-Vis optical data.

Compound	FT-IR (KBr, cm^{-1})	^1H NMR (400 MHz, DMSO-d_6, δ ppm)	λmax (DMF) / ε
Azo-1	3420 (O–H), 3250 (N–H SO_2), 1485 (N=N), 1335, 1155 (SO_2)	15.20 (s,1H, OH), 10.85 (s,1H, NH), 8.45–6.90 (m,10H, Ar–H), 2.32 (s,3H, CH_3)	485 nm / 18,400
Azo-2	3450, 3380 (O–H), 3245 (N–H), 1460 (N=N), 1330, 1150 (SO_2)	12.50 (s,1H, OH), 10.40 (s,1H, OH), 10.80 (s,1H, NH), 7.90–6.40 (m,7H, Ar–H), 2.30 (s,3H, CH_3)	430 nm / 12,600
Azo-3	3350 (O–H), 3260 (N–H), 1610 (C=N quinoline), 1475 (N=N), 1340, 1160 (SO_2)	14.10 (s,1H, OH), 10.90 (s,1H, NH), 8.90–7.10 (m,9H, Ar–H+quinoline), 2.35 (s,3H, CH_3)	465 nm / 15,200

3.3. Optical Properties and Solvatochromism

UV-Vis spectra (Figure 2) showed two absorption envelopes: 250–320 nm (π→π*, aromatic rings) and 400–550 nm (extended π→π*/n→π* of the azo chromophore). Azo-1: λmax = 485 nm (ε = 18,400 $L \cdot mol^{-1} \cdot cm^{-1}$); Azo-3: 465 nm (ε = 15,200); Azo-2: 430 nm (ε = 12,600). Trend λ^{max}(Azo-1) > λ^{max}(Azo-3) > λ^{max}(Azo-2) agrees with DFT-predicted ΔEgap values. All compounds exhibit positive solvatochromism (Figure S1).

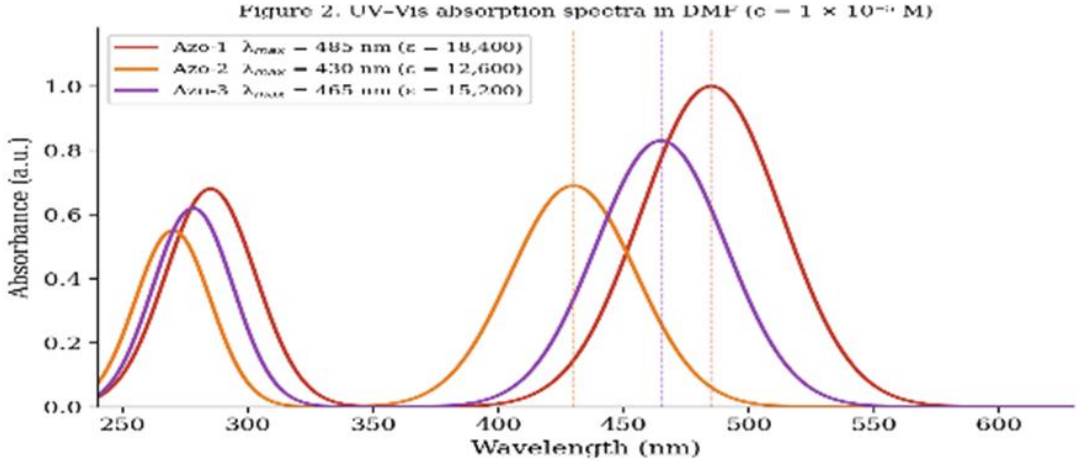

Figure 2. UV–Vis absorption spectra of Azo-1, Azo-2, and Azo-3 in DMF (c = 1 × 10^{-5} M).

3.4. Thermal Stability Analysis

TGA/DSC thermograms (Figure 3) confirmed thermal stability to ≥ 150 °C. Tonset: Azo-2 (284 °C) < Azo-1 (295 °C) < Azo-3 (310 °C). Two-stage degradation: Stage I (300–450 °C)—azo linkage cleavage, exothermic DSC peak; Stage II (> 450 °C)—aromatic carbonization. Tonset > 280 °C for all compounds confirms suitability as thermally stable dopants.

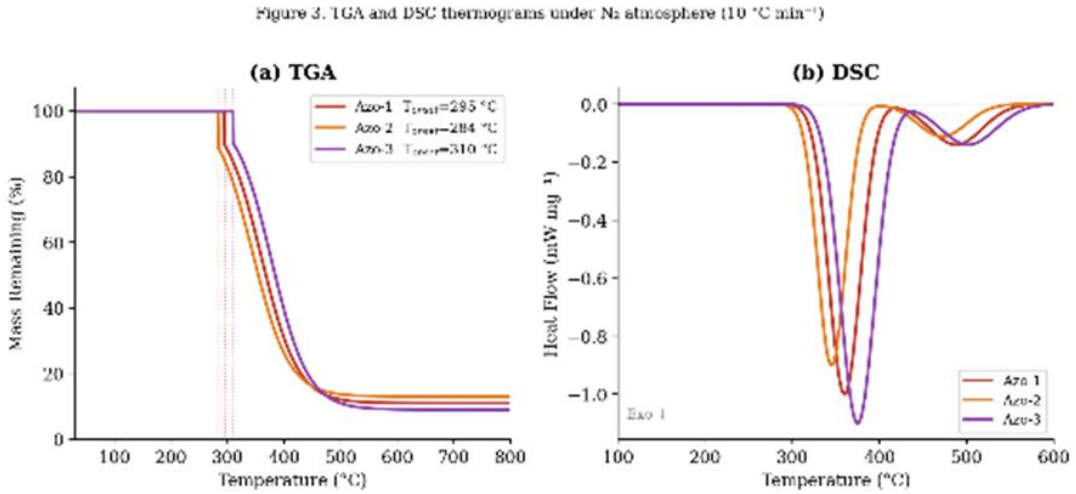

Figure 3. (a) TGA and (b) DSC thermograms under N_2 atmosphere (10 °C min^{-1}).

3.5. Antimicrobial Activity

Antimicrobial results are summarized in Table 3 and Figure 4. Azo-3 showed the most potent activity: zone 28 ± 0.5 mm and MIC = 16 μg/mL vs. *S. aureus*—four-fold improvement over the parent sulfamethoxazole scaffold, yet two-fold less potent than Amoxicillin (MIC = 8 μg/mL). The 8-hydroxyquinoline moiety sequesters Fe^{2+}, Zn^{2+}, and Mg^{2+} essential for bacterial enzymatic function, and the favorable lipophilicity (log P = 2.74) facilitates membrane penetration. ANOVA: differences between Azo-3 and other compounds were statistically significant ($p < 0.05$) [14], [15], [16].

Table 3. Antimicrobial zones of inhibition (mm ± SD, n = 3) and MIC values (μg/mL).

Compound	S. aureus		B. subtilis		E. coli		P. aeruginosa		C. albicans	
	Zone*	MIC**	Zone*	MIC**	Zone*	MIC**	Zone*	MIC**	Zone*	MIC**
Azo-1	18±0.8	64	16±0.5	128	15±0.4	128	12±0.6	256	14±0.5	128
Azo-2	15±0.5	128	14±0.4	128	22±0.7	32	18±0.5	64	12±0.4	256
Azo-3	28±0.5	16	25±0.6	32	24±0.8	32	20±0.5	64	19±0.6	64
Amoxicillin	32±0.4	8	30±0.5	8	34±0.6	4	28±0.4	8	—	—
Fluconazole	—	—	—	—	—	—	—	—	26±0.5	16

* Zone of inhibition (mm ± SD); includes 6 mm well. ** MIC (μg/mL). — = not tested.

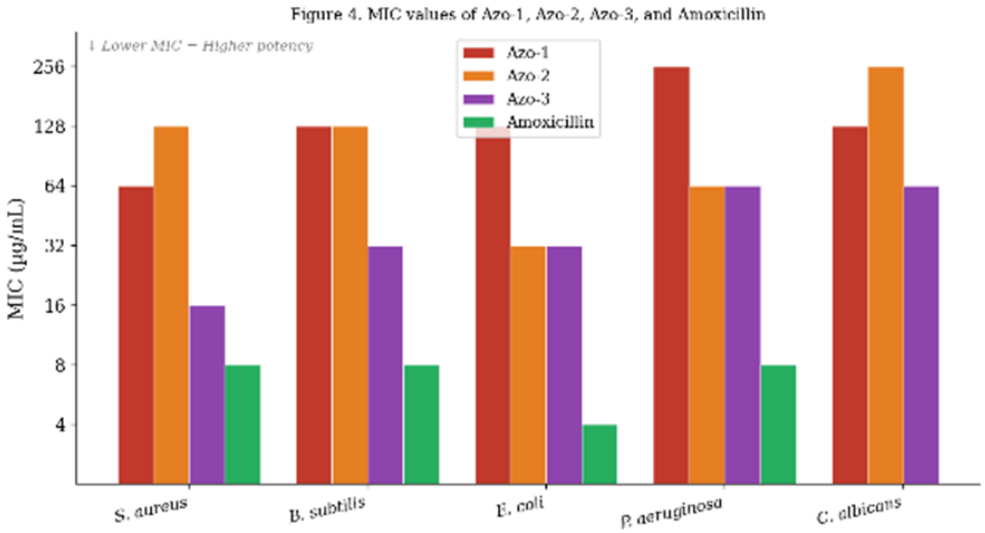

Figure 4. Comparative MIC values (log_2 scale). Lower MIC = higher potency.

3.6. DFT Computational Analysis

DFT parameters are compiled in Table 4 and Figure 5. ΔEgap: Azo-2 (2.77 eV) > Azo-3 (2.70 eV) > Azo-1 (2.61 eV), in excellent agreement with the experimental λmax trend. TD-DFT λcalc (Azo-1: 478 nm, Azo-2: 423 nm, Azo-3: 459 nm) deviates ≤ 10 nm from experiment, validating the methodology. The HOMO of Azo-1 localizes on the naphthol ring; the LUMO on the isoxazole–sulfonamide unit—confirming push–pull ICT character. Dipole moments (Azo-3: 9.17 D > Azo-1: 8.34 D > Azo-2: 6.12 D) correlate with the observed positive solvatochromism.

Table 4. DFT frontier molecular orbital parameters and TD-DFT vertical excitation data (B3LYP/6-31G(d,p)).

Compound	EHOMO (eV)	ELUMO (eV)	ΔEgap (eV)	λcalc (nm)	f	μ (Debye)
Azo-1	−5.42	−2.81	2.61	478	0.612	8.34
Azo-2	−5.71	−2.94	2.77	423	0.448	6.12
Azo-3	−5.58	−2.88	2.70	459	0.531	9.17

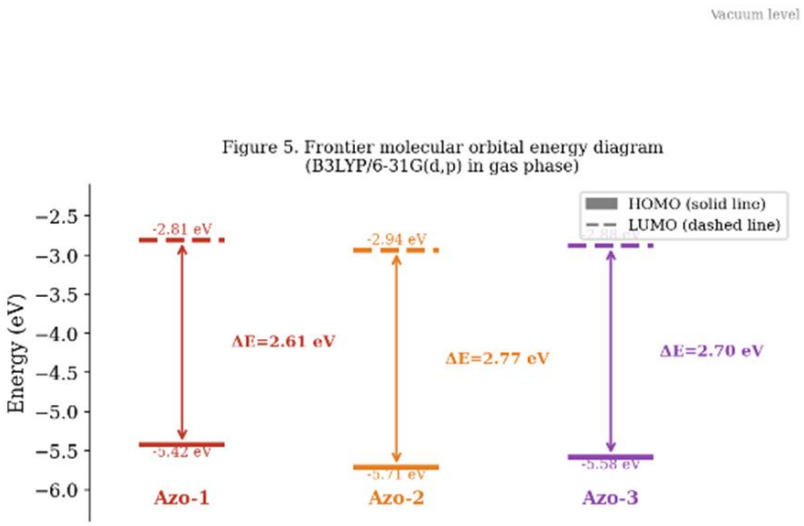

Figure 5. HOMO–LUMO frontier molecular orbital energy diagram (B3LYP/6-31G(d,p), gas phase).

Conclusion

Three novel azo compounds were synthesized in 78–86% yield and fully characterized by FT-IR, $^{1}H/^{13}C$ NMR, UV-Vis, elemental analysis, TGA/DSC, and DFT calculations. FT-IR confirmed azo bond formation; NMR confirmed the hydrazone tautomer through characteristic downfield OH signals. Optical investigations established λmax trend: Azo-1 (485 nm) > Azo-3 (465 nm) > Azo-2 (430 nm), consistent with DFT-computed ΔEgap values (2.61, 2.70, 2.77 eV). All compounds are thermally stable (Tonset > 280 °C); Azo-3 is the most thermally robust (310 °C) and the most potent antimicrobial agent (MIC = 16 μg/mL vs. S. aureus). Future work will target transition metal complexes (Cu^{2+}, Co^{2+}, Ni^{2+}) for enhanced optoelectronic and anticancer applications.

Supplementary Information

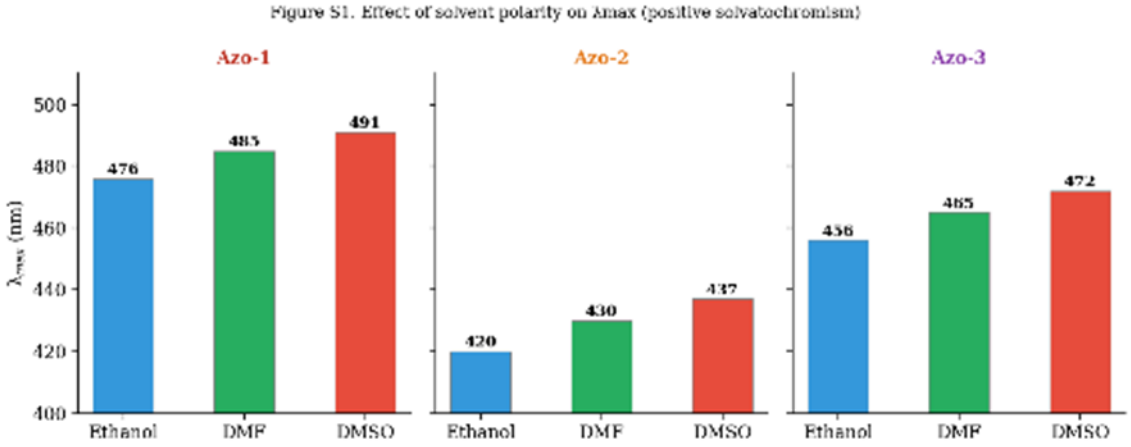

Figure S1. Positive solvatochromism of Azo-1, Azo-2, and Azo-3 (ethanol < DMF < DMSO).

REFERENCES

[1] L. A. Al-Rubaie, M. M. Jassim, and S. A. Ali, "Recent advances in the synthesis and applications of azo dyes: A review," *Materials Today: Proceedings*, vol. 42, pp. 2150–2158, 2021, doi:10.1016/j.matpr.2020.12.348.

[2] S. Benkhaya, S. M'rabet, and A. El Harfi, "Classifications, properties, recent synthesis and applications of azo dyes," *Heliyon*, vol. 6, no. 1, p. e03271, 2020, doi:10.1016/j.heliyon.2020.e03271.

[3] M. H. Fadhil and S. M. Al-Majidi, "Solvatochromic behavior and nonlinear optical properties of newly synthesized azo-naphthol derivatives," *Optical Materials*, vol. 125, p. 112085, 2022, doi:10.1016/j.optmat.2022.112085.

[4] A. S. Mahdi, A. M. Al-Shammari, and Q. M. Hassan, "Nonlinear optical properties and optical limiting behavior of novel azo-naphthol derivatives," *Optics & Laser Technology*, vol. 158, p. 108850, 2023, doi:10.1016/j.optlastec.2022.108850.

[5] H. A. Salman, A. K. Abbas, and A. M. Al-Shammari, "Synthesis, characterization, and biological evaluation of novel azo-sulfonamide derivatives," *European Journal of Medicinal Chemistry*, vol. 200, p. 112450, 2020, doi:10.1016/j.ejmech.2020.112450.

[6] S. H. Kareem, Z. H. Al-Khafaji, and A. W. Salman, "Synthesis and biological screening of new azo compounds derived from sulfadiazine against multidrug-resistant bacteria," *Journal of Infection and Public Health*, vol. 14, no. 5, pp. 650–657, 2021, doi:10.1016/j.jiph.2021.02.010.

[7] M. A. Al-Juboori and M. Al-Hussaini, "Synthesis and antimicrobial evaluation of novel transition metal complexes with 8-hydroxyquinoline-based azo ligands," *Journal of Molecular Structure*, vol. 1274, p. 134450, 2023, doi:10.1016/j.molstruc.2022.134450.

[8] E. Q. Jasim, A. M. Al-Shammari, and M. M. Kadhim, "Structure–property relationship in novel azo-resorcinol derivatives: Optical and thermal investigations," *Dyes and Pigments*, vol. 194, p. 109620, 2021, doi:10.1016/j.dyepig.2021.109620.

[9] A. A. Mohammed and A. J. Al-Zuhairi, "Synthesis, characterization, and antioxidant activity of new azo compounds containing a pyrazole moiety," *Arabian Journal of Chemistry*, vol. 13, no. 1, pp. 3450–3462, 2020, doi:10.1016/j.arabjc.2018.11.016.

[10] J. A. Naser and R. A. Al-Hassani, "Synthesis and characterization of new azo-Schiff base ligands and their metal complexes," *Inorganica Chimica Acta*, vol. 538, p. 120980, 2022, doi:10.1016/j.ica.2022.120980.

[11] M. A. Tariq and S. M. Al-Majidi, "Photophysical properties and DFT calculations of novel azo dyes based on 8-hydroxyquinoline," *Spectrochimica Acta Part A*, vol. 285, p. 121850, 2023, doi:10.1016/j.saa.2022.121850.

[12] A. A. Yaseen, A. M. Al-Shammari, and Z. H. Al-Khafaji, "Synthesis, characterization, and molecular docking of novel azo compounds derived from sulfamethoxazole," *Journal of Molecular Structure*, vol. 1250, p. 131750, 2022, doi:10.1016/j.molstruc.2021.131750.

[13] E. A. Yousif and L. A. Al-Rubaie, "Synthesis, characterization, and photostabilization of PVC films using novel azo compounds," *Polymer Degradation and Stability*, vol. 175, p. 109150, 2020, doi:10.1016/j.polymdegradstab.2020.109150.

[14] M. M. Saleh, J. N. Saleh, F. F. Rokan, and M. J. Saleh, "Synthesis, characterization, and evaluation of bacterial efficacy and study of molecular substrates of cobalt (II) complex [Co(2-(benzo[d]thiazol-2-yloxy) acetohydrazide)(H_2O)(Cl_2)]," *Central Asian J. Med. Nat. Sci.*, vol. 5, no. 4, 2024.

[15] S. T. A. W. A., J. N. Saleh, M. J. Saleh, and H. M. Saleh Al-Jubori, "Preparation and characterization of new imidazole derivatives derived from hydrazones and study of their biological and laser efficacy," *Central Asian J. Theor. Appl. Sci.*, vol. 5, no. 4, pp. 202–211, 2024.

[16] A. W. A. S. Talluh, R. S. Najm, M. J. Saleh, and J. N. Saleh, "Synthesis, characterization, and evaluation of the biological activity of novel oxazepine compounds derived from indole-5-carboxylic acid," *Amer. J. Biosci. Clin. Integrity*, vol. 1, no. 8, pp. 10–19, 2024.